Journal of Non-Crystalline Solids 436 (2016) 44–50

Contents lists available at ScienceDirect

Journal of Non-Crystalline Solids

journal homepage: www.elsevier.com/locate/jnoncrysol

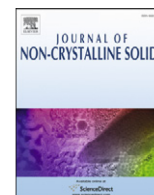

Impact of band tail distribution on carrier trapping in hydrogenated amorphous silicon for solar cell applications

S. Nunomura *, I. Sakata, K. Matsubara

Research Center for Photovoltaics, National Institute of Advanced Industrial Science and Technology, 1-1-1 Umezono, Tsukuba, Ibaraki 305-8568, Japan

A R T I C L E I N F O

Article history:
Received 2 November 2015
Received in revised form 5 January 2016
Accepted 11 January 2016
Available online 12 February 2016

Keywords:
Carrier trapping
Optical pump-probe technique
Hydrogenated amorphous silicon (a-Si:H)
Solar cells
Photocurrent

A B S T R A C T

Carrier trapping in hydrogenated amorphous silicon (a-Si:H) has been investigated by means of an optical pump-probe technique. The trapped carriers (electrons) at the conduction band tail are detected as an increment of the photocurrent, and their density is quantitatively determined under the assumption of carrier generation and recombination kinetics. We find that carrier trapping strongly depends on the band tail distribution in addition to the pump light intensity. Specifically, the trapped electron density increases with the Urbach energy that characterizes the valence band tail broadening. Under the condition of a pump light intensity of 10 mW/cm^2 operated at 532 nm, the trapped electron density is determined to be $\approx 4 \times 10^{17}$ cm^{-3} for an intrinsic a-Si:H film with an Urbach energy of 45 mV. The effects of carrier trapping on the device performance are studied in single-junction a-Si:H p-i-n solar cells. The results suggest that carrier trapping causes a reduction in the fill factor of the solar cells.

© 2016 Elsevier B.V. All rights reserved.

1. Introduction

Carrier trapping is a key factor that restricts carrier transport in amorphous semiconductor devices [1–5]. Once carriers are trapped in those devices, particularly in the active layer, the trapped carriers result in the Shockley–Read–Hall (SRH) recombination [6], and thereby the carrier lifetime is reduced. Besides, an accumulation of trapped carriers induces the quasi-Fermi level shift accompanying band bending [7,8], which may degrade the carrier collection. The carrier trapping thus impacts on the carrier recombination and collection so that studies on carrier trapping are beneficial for understanding the carrier transport and improving the device performance.

In amorphous semiconductors such as hydrogenated amorphous silicon (a-Si:H), carriers can be trapped at gap states (also called localized states) associated with various defects. The gap states are usually classified into two groups: the band tail states and the mid-gap states [9,10]. The band tail states, related to the network disorder, are extended from the conduction and valence band (CB and VB) edges. The CB tail states exhibit electron traps whereas the VB tail states exhibit hole traps [6]. Because of the existence of these traps, the carrier mobility, μ, is strongly limited. On the other hand, the mid-gap states, originating from dangling bonds (DBs), are formed near the middle of bandgap. They behave as recombination centers for carriers. So, the carrier lifetime, τ, is often governed by the density of these mid-gap states [6].

Among amorphous semiconductors, a-Si:H is widely used for various device applications. For example, in thin-film Si solar cells [11,12], an a-Si:H film is used as a photovoltaic layer that plays important roles in carrier transport as well as light absorption. In amorphous/crystalline Si (c-Si) hetero-junction solar cells [13,14], a thin layer of a-Si:H is employed to passivate the c-Si surface and also selectively transfer carriers, i.e., either electrons or holes to electrodes. The passivation and selective transfer are known to be required for this kind of high-efficiency solar cells [15].

So far, carrier trapping in an a-Si:H film has been well studied by time of flight technique [2–5]. The gap states, i.e., the origin of carrier trapping, have been characterized by several methods such as constant photocurrent method (CPM) [16–19], Fourier transform photocurrent spectroscopy (FTPS) [20,21], modulated photocurrent (MPC) spectroscopy [22], and deep level transient spectroscopy (DLTS) [23–25]. Particularly, the density of mid-gap states, related to DBs, have been quantified by electron spin resonance (ESR) [26,27]. Furthermore, the distribution of the mid-gap states is studied by dual-beam photoconductivity (DBP), in which the bias light is used to precisely control the quasi-Fermi level [28]. Nevertheless, the impact of the gap state distribution on carrier trapping and the device performance have not been investigated systematically.

In this paper, we investigate carrier trapping in intrinsic a-Si:H films from the viewpoint of the band tail distribution. The trapped carrier (electron) density at the CB tail are determined quantitatively, using an optical pump-probe technique. This technique has been already applied to in-situ monitoring of film growth processes in a-Si:H [29]. Because of its high sensitivity and convenience, we extend this technique to ex-situ characterization of a-Si:H in this article. One advantage of this technique is that one can evaluate the density of electron traps in the samples with a thickness of up to several hundred nm [29],

* Corresponding author.
E-mail address: s.nunomura@aist.go.jp (S. Nunomura).

http://dx.doi.org/10.1016/j.jnoncrysol.2016.01.021
0022-3093/© 2016 Elsevier B.V. All rights reserved.

which includes the typical thickness in the state-of-art a-Si:H solar cells [11,12]. This is in contrast with the case of time-of-flight technique, where the samples having a thickness of several micron meters are necessary [2–5]. Using this pump-probe technique and CPM, a correlation between the trapped electron density and the VB tail broadening is studied. The effects of carrier trapping on the device performances are examined in a-Si:H p-i-n solar cells.

The paper consists of the following parts. In the next section (Section 2), a theory for carrier generation and recombination is briefly described to derive the trapped carrier density. In experimental section (Section 3), we explain sample preparation, trap characterization techniques, and a-Si:H solar cell structure. In results and discussion (Section 4), the trapped carrier density, the tail state distribution and the device performance are reported. The occupation, the origin of traps, carrier transport and trapping are then discussed. Finally, the solar cell performances are examined in terms of carrier transport and trapping.

2. Theory

The trapped carriers are detected by an optical pump-probe technique, using the experimental setup shown in Fig. 1. The pump generates carriers and fills the traps, whereas the probe emits trapped carriers to the CB (see also Fig. 2(a)). The pump pins the quai-Fermi level that is not influenced by the probe (this will be confirmed in Section 4.1). The generated carriers are collected with contacts and measured as a photocurrent. The photocurrent is slightly increased while a sample is illuminated with the probe in addition to the pump [30]. This increase originates from de-trapping of carriers, and thus trapped carriers are measured as an increment of the photocurrent. We hereafter call it a trap current.

In a steady state, the photo and trap currents, I_p and I_t, are given by

$$I_p = e g_v \tau v_d, \tag{1}$$

$$I_t = e g_t \tau v_d, \tag{2}$$

where e, g_v, g_t, τ, and v_d are the elementary charge, the carrier generation rates under pump and probe illumination (Fig. 2(a)), the recombination lifetime and the drift velocity of carriers, respectively. Here, the recombination is characterized by τ, and is predominated by a trap mediated SRH type [6] for large mid-gap states and tunneling phenomena for large band tail states [9]. For carrier generation, g_v and g_t, are expressed as follows.

$$g_v = n_v \sigma_v \Gamma_{\text{pump}}, \tag{3}$$

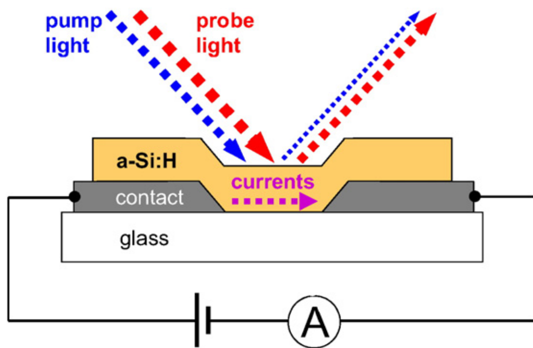

Fig. 1. Schematic view of experimental setup. An a-Si:H film is illuminated with the pump and probe light to induce the photo and trap currents. The pump and probe light intensities are modulated at different frequencies, and the oscillating photo and trap currents are detected with a lock-in technique. The sample structure is a-Si:H film (220 ± 10 nm) on a glass substrate with interdigitated contacts. The contacts are biased at 10 V with respect to each other.

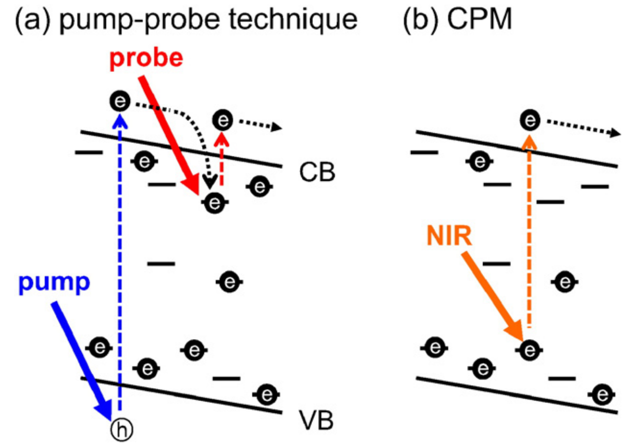

Fig. 2. Carrier dynamics in a pump-probe technique and constant photocurrent method (CPM). (a) In a pump-probe technique, the pump light generates free carriers and fill the traps, whereas the probe light emits trapped carriers (electrons) at the CB tail to the CB. (b) In CPM, quasi-monochromatic near infrared (NIR) light excites electrons at the VB tail to the CB.

$$g_t = n_t \sigma_t \Gamma_{\text{probe}}, \tag{4}$$

where, n_v, n_t, σ_v, σ_t, Γ_{pump}, and Γ_{probe} are the densities of the valence and trapped carriers (electrons), the photoabsorption cross sections of the valence and trapped carriers (electrons), and the photon fluxes of the pump and probe light, respectively. Dividing I_t by I_p, the trapped carrier density, n_t, is derived as follows.

$$n_t = \frac{\sigma_v \Gamma_{\text{pump}}}{\sigma_t \Gamma_{\text{probe}}} \frac{I_t}{I_p} n_v. \tag{5}$$

We remark here that n_t is not a function of τ since it is canceled out when dividing I_t by I_p. For convenience, we normalize n_t by n_v. The normalized trapped carrier density, n_t/n_v, is thus given by

$$n_t/n_v = \frac{\sigma_v}{\sigma_t} \frac{\Gamma_{\text{pump}}}{\Gamma_{\text{probe}}} \frac{I_t}{I_p}. \tag{6}$$

In this study, we assume $\sigma_v/\sigma_t = 1$ since the optical matrix elements of a-Si:H films are less-dependent on the photon energy in a range of $h\nu = 0.6$ to 3.0 eV [31]. A similar assumption is also described in Ref. [32] for examining the sub-gap absorption spectra. The pump and probe photon energies used in this study are included in this range, described later (Section 3.2).

3. Experimental

3.1. Preparation of a-Si:H films

In order to demonstrate the usefulness of the optical pump-probe technique for evaluating the density of trapped electrons in a-Si:H, we have applied this technique to a series of a-Si:H samples where the growth temperature was varied. Intrinsic a-Si:H films were prepared on glass substrates by means of plasma enhanced chemical-vapor-deposition (PECVD), at various growth temperatures of T_g = 373 K–593 K. Our PECVD was operated using a 60 MHz capacitively-coupled discharge of a hydrogen (H_2) and silane (SiH_4) gas mixture in parallel-plate configuration. The gas mixture was introduced from the powered (PWD) electrode showerhead; the H_2 and SiH_4 flow rates were 50 sccm and 10 sccm, respectively. The discharge was sustained between the PWD and electrically grounded (GND) electrodes by applying a voltage of 35 V peak to peak at a pressure of 0.3 Torr. The electrode gap was set at 22 mm. We placed a glass substrate on the GND

electrode that was heated at a given T_g. An a-Si:H film was grown on the substrate at a rate of 0.23 ± 0.04 nm/s, and the thickness was controlled at 220 ± 10 nm by adjusting the growth period. Details for our PECVD setup are described elsewhere [33–35].

3.2. Photo and trap current measurements

We measured I_p and I_t in an a-Si:H film under pump and probe light, as shown in Fig. 1. Two lasers were used as light sources: a 532 nm visible laser ($h\nu_{pump} = 2.33$ eV) operated at a continuous-wave (CW) output power of 10 mW ($\Gamma_{pump} = 2.7 \times 10^{16}$ photons/cm^{2}s) for the pump and a 1342 nm near-infrared laser ($h\nu_{probe} = 0.92$ eV) at a CW output power of 500 mW ($\Gamma_{probe} = 3.4 \times 10^{18}$ photons/cm^{2}s) for the probe. The pump and probe photon energies are thus chosen to satisfy $h\nu_{pump} > E_g > h\nu_{probe}$, where E_g is the optical bandgap. The intensities of these light, P_{pump} and P_{probe}, were adjusted with neutral density filters. Both the pump and probe light were superposed on an a-Si:H film with an area of ≈ 1 cm^2 at a incident angle of 85°. The generated carriers were then collected with a pair of the interdigitated contacts, which yielded the currents, I_p and I_t. Since these currents are dominated by the electron current rather than the hole current [36], trapped carriers detected with this technique are regarded as trapped electrons. The contacts were made of Ag covered with 40 nm-thick Ga-doped ZnO, and were biased at 10 V with respect to each other. The interdigitated contacts provided nineteen channels. The dimensions of each channel were 0.2 mm in length and 5 mm in width. All the channels were included in the illuminated area.

Because I_t was rather small compared with I_p, we used a lock-in technique to distinguish I_t from I_p. The pump and probe light were modulated at 1.001 kHz and 0.999 kHz, and the currents oscillating at these two frequencies were extracted using a lock-in amplifier with a time constant of 100 ms. We confirmed that I_t was less-dependent on the chopping frequency from 10 to 1.0 kHz; it was varied by $\pm 20\%$, due to the probe light intensity overshoot. With the measured I_p and I_t, the trapped carrier density was calculated from Eq. (5).

3.3. Gap state characterization

The gap state distribution was measured by using an established technique of CPM [16–19]. The samples evaluated with CPM were those used for detection of trapped carriers. In CPM, an a-Si:H film on the glass substrate was illuminated with quasi-monochromatic near infrared (NIR) light to excite electrons at the VB tail to the CB, as shown in Fig. 2(b). The excited electrons were then collected with contacts, and measured as a sub-gap absorption current. The current was maintained constant while scanning the wavelength of NIR light to keep the electron lifetime. For our samples, the current was fixed at 0.5 pA by adjusting the intensity of NIR light. A sub-gap absorption spectrum, i.e., a CPM spectrum, was thus obtained via the wavelength scan in a range of 700 nm to 1300 nm (i.e., the photon energy between 1.03 eV and 1.77 eV). The spectrum was quantified using an absorption coefficient, α, at 1.77 eV, determined from spectroscopic ellipsometry (SE) under the assumption of the Tauc–Lorentz model [39,40].

The gap-state distribution was characterized by two parameters obtained from a CPM spectrum: the Urbach energy [41] and the density of mid-gap states [9,10]. The Urbach energy, E_U, i.e., a measure for the VB tail broadening, was calculated from an exponential decay of the spectrum in a range from 1.45 eV to 1.75 eV. The density of mid-gap states was evaluated with the absorption coefficient at 1.2 eV, $\alpha_{1.2eV}$. This $\alpha_{1.2eV}$ is known to reflect the density of mid-gap states, and increases linearly with the density of DBs, n_{DB} [42,43]. To quantitatively determine n_{DB}, we carried out a ESR measurement for an 220 nm-thick a-Si:H film prepared on a quartz glass at $T_g = 473$ K. In ESR measurement [26,27], the microwave absorption at g-value of 2.0055 was measured under magnetic field. The absolute value of n_{DB} was deduced from the absorption, comparing with that of a controlled sample, in which the DB density was known.

3.4. A-Si:H p-i-n solar cells

Single-junction a-Si:H p-i-n solar cells were prepared to study the correlation between carrier trapping and solar cell performance. We fabricated solar cells on textured glass substrates (Asahi U-type) with a following structure: a glass substrate/F-doped SnO_2/p-layer(a-SiC:H 10 nm)/i-layer(a-Si:H 220 nm)/n-layer(μc-Si:H 30 nm)/Ga-doped ZnO(40 nm)/Ag(200 nm). In these solar cells, the i-layer of a-Si:H was grown at various T_g of 373 K - 553 K to change the carrier transport and trapping. The deposition of i-layer at different T_g may affect the p-layer and p-i interface properties in such a super-straight structure; nevertheless the cell performance is primarily governed by carrier transport and trapping in the i-layer. The active area of solar cells was 0.25 cm^2. The solar cell performance was measured at standard test conditions: air mass (AM) 1.5, 100 mW/cm^2 irradiation at 25 °C.

4. Results and discussion

4.1. Occupation of traps

The occupation of traps is studied by changing P_{pump} in our pump-probe experiments. Fig. 3 shows P_{pump}-dependence of I_p, I_t and n_t/n_v in an a-Si:H film grown at $T_g = 473$ K. As apparent, I_p is proportional to P_{pump} in a wide range of P_{pump}, whereas I_t shows a tendency to be gradually saturated at high intensities, $P_{pump} \gtrsim 1$ mW. Correspondingly, n_t/n_v, calculated from Eq. (6) with a ratio of I_t to I_p, shows a similar tendency to I_t on P_{pump}. Such a tendency indicates that carriers are populated more at higher P_{pump}, and thus the trap occupation is gradually increased.

The occupation is not influenced by illumination of the probe light ($P_{probe} \lesssim 500$ mW). This is indicated by a linear relationship between I_t and P_{probe}, as shown in Fig. 4. According to Eq. (5), I_t is expected to increase linearly with P_{probe} while the occupation, i.e., n_t remains constant. If a large amount of carriers are de-trapped under high-P_{probe} conditions, I_t should be lowered; it is, however, not observed in our case, as in Fig. 4.

4.2. Origin of trapped carriers

The origin of trapped carriers (electrons) can be deduced from evaluating a quantitative value of n_t, and comparing it with the densities of the mid-gap and CB tail states. As shown in Fig. 3, n_t/n_v is obtained to be

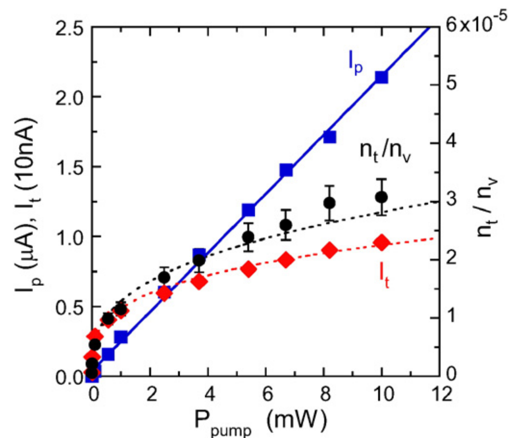

Fig. 3. Photocurrent, I_p, trap current, I_t, and normalized trapped carrier density, n_t/n_v, as a function of pump light intensity, P_{pump}. I_p increases linearly with P_{pump}, whereas I_t and n_t/n_v shows a tendency to be gradually saturated at high P_{pump}. The solid line is the best linear fit of I_p. The dotted lines are guides to the eyes.

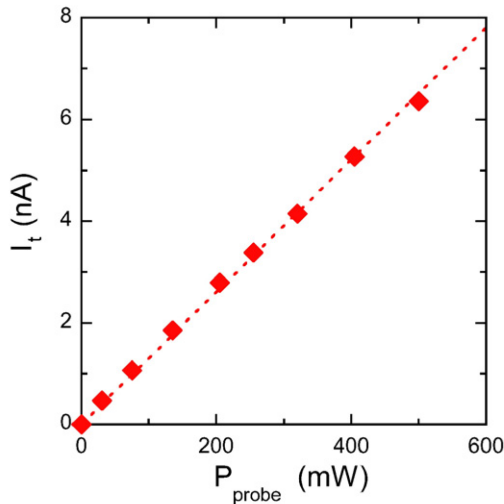

Fig. 4. I_t as a function of probe light intensity, P_{probe}. I_t increases linearly with P_{probe}. The dashed line denotes the linear fit.

$\approx 3 \times 10^{-5}$ for an a-Si:H film grown at $T_g = 473$ K under an illumination condition of $P_{pump} = 10$ mW. Taking the averaged density of VB states, 2×10^{22} cm^{-3} eV^{-1} [31], and considering the energy width for electron excitation by the pump ($h\nu_{pump}$-$E_g = 2.33 - 1.73 = 0.6$ eV), we estimate $n_v = 1.2 \times 10^{22}$ cm^{-3}. With this value of n_v, we determine $n_t \approx 4 \times 10^{17}$ cm^{-3} from Eq. (5).

For the density of mid-gap states, we regard it as n_{DB}. Our ESR measurement gives $n_{DB} = 4.9 \pm 0.5 \times 10^{16}$ cm^{-3} for the film yielding above mentioned n_t. As for the upper limit of the density of the CB tail states, n_{tail}, it is known to be roughly 10^{19} cm^{-3} [44]. Therefore, we notice a relation, $n_{DB} < n_t < n_{tail}$. This relation confirms that carrier trapping takes places mainly at the CB tail states rather than the mid-gap states. In addition, the value of n_t determined in this analysis is consistent with the density of state distribution in the CB tail of a-Si:H, obtained with MPC spectroscopy [22].

4.3. Carrier transport and trapping

Here, we describe carrier transport and trapping in a-Si:H films grown at various T_g. The carrier transport, which is often characterized by the μ-τ product, is evaluated with I_p under the condition of constant g_v since $I_p \propto g_v\mu\tau$ [36]. Fig. 5 shows I_p, I_t and n_t/n_v as a function of T_g. As shown, I_p is broadly peaked around $T_g = 493$ K, and significantly

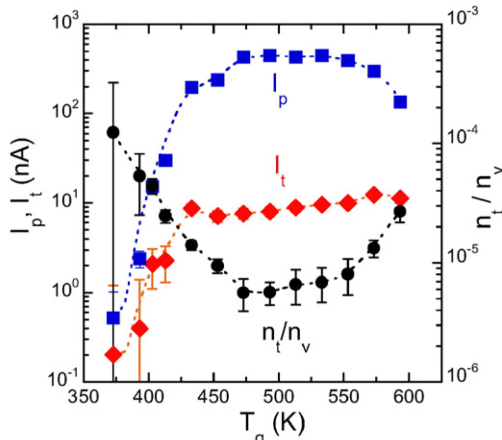

Fig. 5. I_p, I_t and n_t/n_v in intrinsic a-Si:H films grown at various growth temperature, T_g. n_t/n_v in a-Si:H films is lowered around $T_g = 493$ K, at which I_p is maximized. Both I_p and I_t are significantly increased with T_g in $T_g \lesssim 433$ K. The dotted lines are guides to the eyes.

reduced at low T_g ($T_g \lesssim 433$ K). On the other hand, I_t shows a tendency different from that of I_p, particularly in high $T_g \gtrsim 433$ K; it increases gently with T_g. Comparing I_t with I_p, we confirm that at I_t typically corresponds to a few percent of I_p. Typical values of I_p and I_t are 500 nA and 10 nA for a film prepared around $T_g = 493$ K under our illumination conditions.

We find that n_t/n_v is minimized for a film prepared around $T_g = 493$ K. The lowest value of n_t/n_v is determined to be $\approx 5 \times 10^{-6}$ under relatively weak illumination of $P_{pump} = 0.4$ mW. An a-Si:H film showing the lowest n_t yields the highest I_p. This correspondence confirms that the highest carrier transport is achieved when carrier trapping is minimized.

4.4. Gap state distribution

The sub-gap absorption spectra of a-Si:H films grown at three different T_g are shown in Fig. 6. As expected [16–19], two prominent features are distinguished: exponential decay in a range of the photon energy from ≈ 1.45 to ≈ 1.75 eV and a broad peak around 1.2 eV. The exponential decay, related to the VB tail, is characterized by E_U. As shown in Fig. 7(a), E_U ranges from ≈ 40 meV to ≈ 65 meV. It is minimized around $T_g = 493$ K, which agrees with a well known optimal temperature for a-Si:H growth reported in early works [37,38]. Errors in E_U are relatively large because of an interference observed in the sub-gap absorption spectra.

The broad peak around 1.2 eV in Fig. 6 reflects the existence of the mid-gap states, as described in Section 3.3. The density of these states is evaluated with $\alpha_{1.2eV}$, as shown in Fig. 7(b). Our films have $\alpha_{1.2eV}$ from ≈ 0.3 cm^{-1} to ≈ 10 cm^{-1}, depending on T_g. The obtained $\alpha_{1.2eV}$ is lowered around $T_g = 473$ K, which is consistent with other experiments performed in early works [19]. However, $\alpha_{1.2eV}$ values of our films grown at low T_g ($T \lesssim 433$ K) are relatively small, compared with those of films prepared by 13.6 MHz radio frequency discharges [19]. This may reflect the effect of low ion bombardment during a-Si:H growth by a 60 MHz very high frequency discharge. The energy of ion bombardment is known to be significantly reduced with increasing

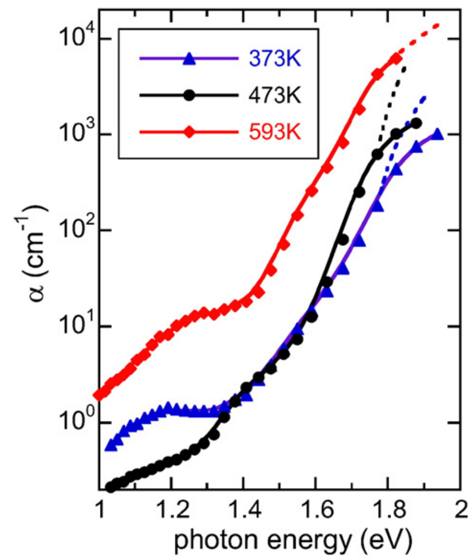

Fig. 6. CPM spectra for a-Si:H films grown at various T_g. The absorption coefficient, α, is plotted as the photon energy. Two prominent features are distinguished: exponential decay in a range of the photon energy from ≈ 1.45 to ≈ 1.75 eV and a broad peak around 1.2 eV. The solid lines are guides to the eyes. The dashed lines denote α determined from spectroscopic ellipsometry (SE) under the assumption of the Tauc–Lorentz model. The solid (CPM spectra) and dashed (SE yielded spectra) lines are relatively smoothly connected at 1.77 eV. The deviation from the solid curve at ≥ 1.77 eV indicates saturation of the sub-gap absorption current due to the surface recombination effects.

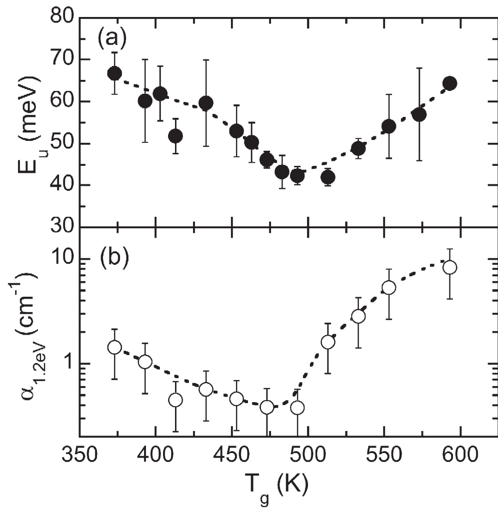

Fig. 7. (a) Urbach energy, E_U, and (b) absorption coefficient at 1.2 eV, $\alpha_{1.2eV}$, as a function of T_g. E_U is ranged from ≈40 meV to ≈65 meV, and minimized around $T_g = 493$ K. (b) $\alpha_{1.2eV}$ is ranged from ≈0.3 cm^{-1} to ≈10 cm^{-1} for a-Si:H films grown at $T_g = 373$ K to 593 K. The dotted lines are guides to the eyes.

the discharge frequency [45], and thereby the DB defect creation is suppressed.

4.5. Gap states and carrier trapping

Now, we describe correlations among $\alpha_{1.2eV}$, n_t/n_v and E_U to discuss the carrier trapping in terms of the band tail distribution. As shown in Fig. 8(a), $\alpha_{1.2eV}$ is increased with E_U, however it shows two different tendencies, i.e., steep and gentle slopes with respect to E_U, depending on T_g. The steep slope is obtained for a-Si:H films prepared at $T_g \gtrsim 493$ K whereas the gentle slope is for those grown at $T_g \lesssim 493$ K. This result indicates that the mid-gap states are created more for a-Si:H films grown at higher T_g compared with those grown at lower T_g even though the VB tail distribution is formed similarly. This is probably related to hydrogen desorption from the growing surface under PECVD [46]. The hydrogen desorption is known to be prominent at high-T_g, which leaves DB defects in the surface and bulk film [26,27], and thus more the mid-gap states are formed.

Our main finding in this study is a nice correlation between n_t/n_v and E_U, as shown in Fig. 8(b). We find that n_t/n_v increases monotonically with E_U; n_t/n_v varies from $\approx 5 \times 10^{-6}$ at $E_U \approx 40$ meV to $\approx 1.5 \times 10^{-4}$ at $E_U \approx 65$ meV. Since n_t/n_v is strongly correlated with E_U, sharpening of the band tail distribution is very efficient for reducing the trapped carriers. Besides, such a nice correlation between n_t/n_v and E_U agrees with the previous results [47], where the characteristic energy of CB tail states and that of the VB tail states are closely related to each other. It should be mentioned, however, that the characteristic energy of CB tail states is evaluated from the thin-film transistor analysis [47], and thus this value reflects the a-Si:H properties near the gate insulator/a-Si:H interface. On the other hand, the relationship between n_t/n_v and E_U obtained in the present paper reflects the bulk properties of a-Si:H films.

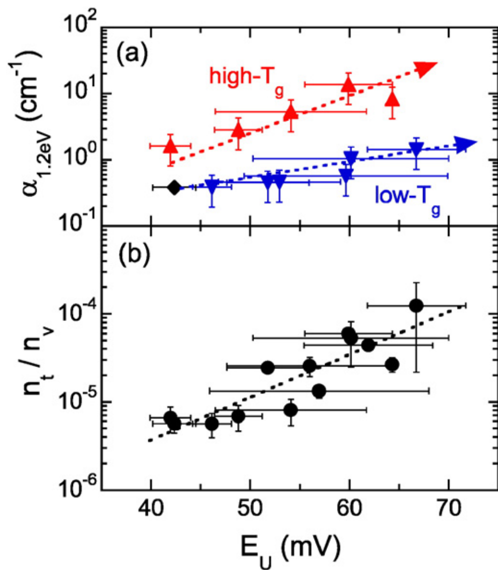

Fig. 8. $\alpha_{1.2eV}$ and n_t/n_v as a function of E_U. (a) $\alpha_{1.2eV}$ increases with E_U, however it shows two different tendencies, i.e., two slopes with respect to E_U, depending on T_g. The steep slope, indicated by the upper dotted arrow, is obtained for a-Si:H films prepared at $T_g \gtrsim 493$ K, whereas the gentle slope, indicated by the lower dotted arrow, is for those grown at $T_g \lesssim 493$ K. The diamond symbol denotes $\alpha_{1.2eV}$ obtained at $T_g = 493$ *K*, where n_t/n_v is minimized. (b) n_t/n_v increases monotonically with E_U. n_t/n_v varies from $\approx 5 \times 10^{-6}$ at $E_U \approx 40$ meV to $\approx 1.5 \times 10^{-4}$ at $E_U \approx 65$ meV. The dotted lines are guides to the eyes.

4.6. Carrier trapping and solar cell performances

In this section, we show the influence of carrier trapping on the solar cell performance. As described in Section 3.4, we prepared a-Si:H p-i-n solar cells, in which the i-layer of a-Si:H was grown at various T_g to change the gap state distribution, and thus n_t in the i-layer. Fig. 9 shows the solar cell performances as a function of T_g. Here, E_g of a-Si:H i-layer, determined from SE under the assumption of the Tauc–Lorentz model [39,40], is also shown. As apparent, the short circuit current, J_{sc}, is gradually increased with T_g. This is primarily due to the effect of bandgap narrowing (see Fig. 9(a) and (b)). The open circuit voltage, V_{oc}, is maximized around $T_g = 453$ K. A large drop in V_{oc} at $T \lesssim 453$ K presumably originates from the limited carrier transport, indicated by I_p in

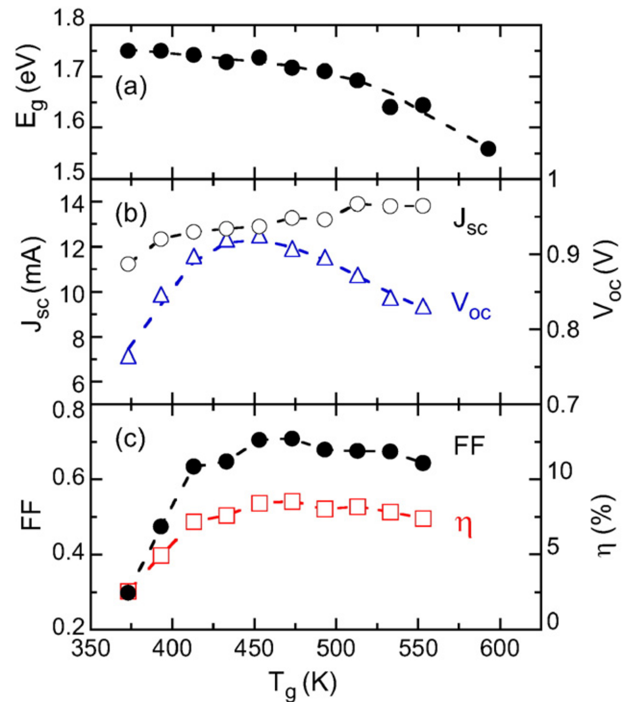

Fig. 9. Optical band gap, E_g, and solar cell performances as a function of T_g. (a) E_g decreases from 1.75 eV at $T_g = 373$ K to 1.55 eV at $T_g = 593$ K. (b) The short circuit current, J_{sc}, is gradually increased with T_g, originating from the effect of bandgap narrowing. The open circuit voltage, V_{oc}, is maximized around $T_g = 453$ K. (c) The fill factor, *FF*, and the efficiency, η, are broadly peaked around $T_g = 473$ K. The highest *FF* and η are 0.71 and 8.6%, respectively. The dashed lines are guides to the eyes.

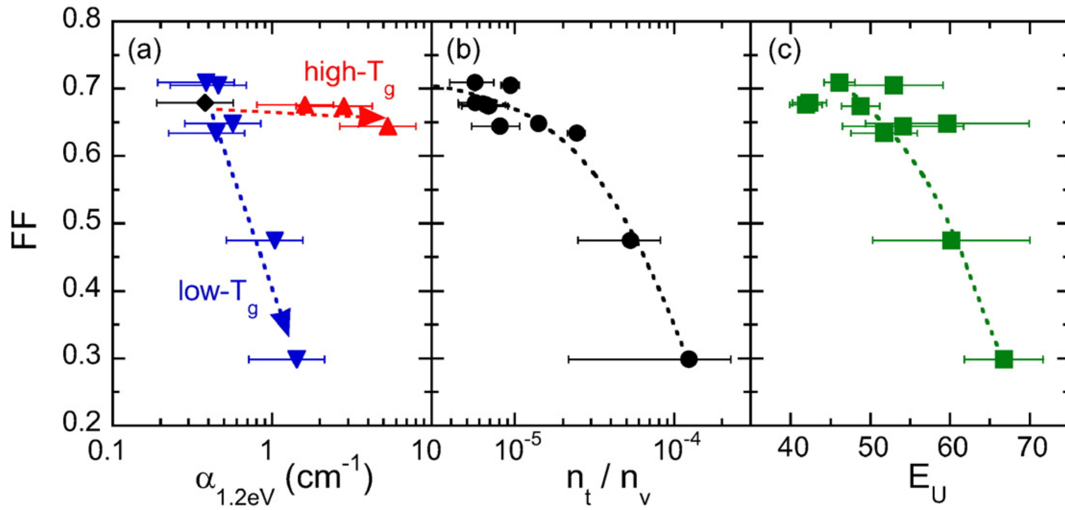

Fig. 10. *FF* vs. $\alpha_{1.2eV}$, n_t/n_v and E_U. (a) *FF* is strongly dependent on $\alpha_{1.2eV}$ only for films grown at $T_g \lesssim 493$ K. It is, however, less-dependent on T_g in $T_g \gtrsim 493$ K. A value of *FF* obtained at $T_g = 493$ K, where n_t/n_v is minimized, is denoted by the diamond symbol. (b) *FF* has a nice correlation to n_t/n_v, i.e. trapped electrons at the CB tail. *FF* reduces from $\approx$0.7 at $n_t/n_v \approx 5 \times 10^{-6}$ to $\approx$0.3 at $n_t/n_v \approx 10^{-4}$. (c) *FF* is correlated to E_U, i.e., the VB tail broadening, relented to the hole trapping. *FF* monotonically reduces with increasing E_U from $\approx$40 meV to $\approx$65 meV. The dotted lines are guides to the eyes.

Fig. 5. A relatively small drop in V_{oc} at $T \gtrsim 453$ K is due to the effect of bandgap narrowing, shown in Fig. 9(a).

The fill factor, *FF*, and the efficiency, η, are broadly peaked around $T_g = 473$ K, as shown in Fig. 9(c). The highest *FF* and η obtained in this study are 0.71 and 8.6%, respectively. According to the device physics and simulation [7,8], *FF* is expected to depend on the density of the mid-gap states and the trapped carriers (electrons and holes). So, we prepare three plots to examine the relations among these parameters: *FF* vs. $\alpha_{1.2eV}$ for examining the effect of mid-gap states, *FF* vs. n_t/n_v for examining the trapped electrons, and *FF* vs. E_U for examining the trapped holes. As shown in Fig. 10(a), *FF* is strongly dependent on $\alpha_{1.2eV}$ only for films grown at $T_g \lesssim 493$ K; it is, however, not for $T_g \gtrsim 493$ K. On the contrary, *FF* is nicely correlated to n_t/n_v, i.e. trapped electrons at the CB tail; *FF* monotonically decreases from $\approx$0.7 at $n_t/n_v \approx 5 \times 10^{-6}$ to $\approx$0.3 at $n_t/n_v \approx 10^{-4}$, as shown in Fig. 10(b). Furthermore, *FF* shows a clear correlation to E_U, i.e., a measure for the VB tail broadening, closely related to hole trapping, as shown in Fig. 10(c). *FF* decreases with increasing E_U from $\approx$40 meV to $\approx$65 meV.

As a result of these correlations, we consider that a reduction in *FF* is affected by carrier trapping at the band tail of the a-Si:H i-layer. As described in Section 1, carrier trapping enhances the SRH type recombination. Besides, the accumulation of trapped carriers in the i-layer induces the band bending, which limits the carrier transport and collection. Such effect is demonstrated in early simulation works [7], in which the space charge density of the order of 10^{16} cm^{-3} is found to significantly modify the electric field distribution and thus degrade the carrier transport in a-Si:H solar cells. In fact, a value of $n_t \approx 4 \times 10^{17}$ cm^{-3} determined in this study is large enough for locally modifying the electric field, and thus reducing the carrier transport in a-Si:H solar cells. It should be mentioned that our data suggests $n_t/n_v \lesssim 10^{-5}$ and/or $E_U \lesssim 45$ meV in order to improve the carrier transport, and thus to achieve high *FF* and η. To distinguish the effects of electron and hole trapping in determining *FF*, further investigations are required.

5. Conclusions

The carrier trapping in a-Si:H films, prepared by PECVD, was investigated from the viewpoint of the gap state distribution. We detected the trapped carriers (electrons) as an increment of the photocurrent using an optical pump-probe technique. The trapped carrier density was determined quantitatively from the photocurrent increment under the assumption of carrier generation and recombination kinetics. It was found that under a pump intensity of 10 mW/cm^2, the trapped electron density was typically $\approx 4 \times 10^{17}$ cm^{-3} for a device-grade intrinsic a-Si:H film with the Urbach energy of 45 mV. Comparing this value to the density of gap state distribution, electron trapping was recognized to take place mainly at the CB tail states. The occupation of the CB tail states was confirmed to increase gradually with the pump light intensity.

We found that in a-Si:H films, carrier trapping was strongly influenced by the band tail broadening. A clear correlation was obtained between the trapped electron density at the CB tail and the Urbach energy, reflecting the exponential energy distribution of the VB tail states. Therefore, the trapped electron density at the CB-tail and VB tail states were related each other, and these were varied by the growth temperature of a-Si:H under PECVD. For an a-Si:H film grown at 493 K, the trapped electron density was minimized, and thereby the carrier transport was maximized.

The influence of carrier trapping on device performance was examined in a-Si:H solar cells. Increasing trapped carriers associated with the band tail broadening in the a-Si:H active layer resulted in lowering the fill factor and the efficiency. Our results suggested that normalized trapped carrier density should be $\lesssim 10^{-5}$ and/or the Urbach energy should be $\lesssim$45 meV to improve the fill factor, and thus to achieve a high efficiency.

Acknowledgments

The authors are grateful to Dr. M. Lozac'h (AIST), Dr. T. Matsui (AIST), and Prof. M. Shiratani (Kyushu Univ.) for their encouragement and valuable comments. This work was supported by JSPS KAKENHI (Grant Numbers 24540546 and 15K04717) and New Energy and Industrial Technology Development Organization (NEDO).

References

[1] P.G. Le Comber, W.E. Spear, Phys. Rev. Lett. 25 (1970) 509.
[2] G. Pfister, H. Scher, Adv. Phys. 27 (1978) 5747.
[3] J.M. Hvam, M.H. Brodsky, Phys. Rev. Lett. 46 (1980) 371.
[4] R.A. Street, Appl. Phys. Lett. 41 (1982) 1060.
[5] W.E. Spear, J. Non-Cryst. Solids 59 (1983) 1.
[6] D.K. Schroder, Semiconductor Material and Device Characterization, John Wiley, Chichester, 2006.
[7] M. Hack, M. Shur, J. Appl. Phys. 58 (1985) 997.
[8] P. Chatterjee, J. Appl. Phys. 76 (1994) 1301.
[9] R.A. Street, Hydrogeneted Amorphous Silicon, Cambridge University Press, Cambridge, 1991.

[10] K. Tanaka, E. Maruyama, T. Shimada, H. Okamoto, Amorphous Silicon, John Wiley, Chichester, 1999.
[11] A. Shah, E. Moulin, C. Ballif, Sol. Energy Mater. Sol. Cells 119 (2013) 311.
[12] B. Rech, H. Wagner, Appl. Phys. A Mater. Sci. Process. 69 (1999) 155.
[13] K. Masuko, M. Shigematsu, T. Hashiguchi, D. Fujishima, M. Kai, N. Yoshimura, T. Yamaguchi, Y. Ichihashi, T. Mishima, N. Matsubara, T. Yamanishi, T. Takahama, M. Taguchi, E. Maruyama, S. Okamoto, IEEE J. Photovolt. 4 (2014) 1433.
[14] M. Schmidt, L. Korte, A. Laades, R. Stangl, Ch. Schubert, H. Angermann, E. Conrad, K.v. Maydell, Thin Solid Films 515 (2007) 7475.
[15] S. De Wolf, A. Descoeudres, Z.C. Holman, C. Ballif, Green 2 (2012) 7.
[16] S. Lee, M. Gunes, C.R. Wronski, N. Maley, M. Bennett, Appl. Phys. Lett. 59 (1991) 1579.
[17] M. Vanecek, J. Kocka, A. Poruba, A. Fejfar, J. Appl. Phys. 78 (1995) 6203.
[18] N. Wyrsch, F. Finger, T.J. McMahon, M. Vanecek, J. Non-Cryst. Solids 137 (1991) 347.
[19] I. Sakata, M. Yamanaka, S. Numase, Y. Hayashi, J. Appl. Phys. 71 (1992) 4344.
[20] J.W. Tomm, A. Jaeger, A. Barwolff, T. Elsaesser, Appl. Phys. Lett. 71 (1997) 2233.
[21] M. Vanecek, A. Poruba, Appl. Phys. Lett. 80 (2002) 719.
[22] K. Hattori, Y. Adachi, M. Anzai, H. Okamoto, Y. Hamakawa, J. Appl. Phys. 76 (1994) 2841.
[23] D.V. Lang, J.D. Cohen, J.P. Harbison, Phys. Rev. B 25 (1982) 5285.
[24] V. Nadazdy, R. Durny, E. Pincik, Phys. Rev. Lett. 78 (1997) 1102.
[25] R. Darwich, J. Non-Cryst. Solids 411 (2015) 119.
[26] S. Yamasaki, U.K. Das, T. Yasuda, J. Non-Cryst. Solids 299 (2002) 185.
[27] U.K. Das, T. Yasuda, S. Yamasaki, Phys. Rev. B 63 (2001) 245204.
[28] S. Lee, M. Gunes, C.R. Wronski, N. Maley, M. Bennett, Appl. Phys. Lett. 59 (1991) 1578.
[29] S. Nunomura, I. Sakata, AIP Adv. 4 (2014) 097110.
[30] S. Nunomura, X. Che, S.R. Forrest, Adv. Mater. 26 (2014) 7555.
[31] W.B. Jackson, S.M. Kelso, C.C. Tsai, J.W. Allen, S.-J. Oh, Phys. Rev. B 31 (1985) 5187.
[32] F. Orapunt, S.K. O'Leary, Solid State Commun. 151 (2011) 411.
[33] S. Nunomura, I. Yoshida, M. Kondo, Jpn. J. Appl. Phys. 49 (2010) 106102.
[34] S. Nunomura, M. Kondo, J. Appl. Phys. 102 (2007) 093306.
[35] S. Nunomura, M. Kondo, H. Akatsuka, Plasma Sources Sci. Technol. 15 (2006) 783.
[36] W. Luft, Y.S. Tsuo, Hydrogenated Amorphous Silicon Alloy Deposition Processes, Marcel DEkker, Inc., New York, 1993.
[37] Z.E. Smith, S. Wagner, Phys. Rev. Lett. 59 (1987) 688.
[38] M. Stutzmann, Philos. Mag. B 60 (1989) 531.
[39] I. An, H.V. Nguyen, N.V. Nguyen, R.W. Collins, Phys. Rev. Lett. 65 (1990) 2274.
[40] H. Fujiwara, Y. Toyoshima, M. Kondo, A. Matsuda, Phys. Rev. B 60 (1999) 13598.
[41] F. Urbach, Phys. Rev. 92 (1953) 1324.
[42] Z.E. Smith, V. Chu, K. Shepard, S. Aljishi, D. Slobodin, J. Kolodzey, S. Wagner, T.L. Chu, Appl. Phys. Lett. 50 (1987) 1521.
[43] J.A. Schmidt, R. Arce, R.H. Buitrago, R.R. Koropecki, Phys. Rev. B 55 (1996) 9621.
[44] R.A. Street, Philos. Mag. B 60 (1989) 213.
[45] S. Nunomura, M. Kondo, Appl. Phys. Lett. 93 (2008) 231502.
[46] Y. Toyoshima, K. Arai, A. Matsuda, K. Tanaka, Appl. Phys. Lett. 56 (1990) 1540.
[47] S. Sherman, S. Wagner, R.A. Gottscho, Appl. Phys. Lett. 69 (1996) 3242.